A numerical method for large-eddy simulation in complex geometries

Krishnan Mahesh
University of Minnesota
George Constantinescu & Parviz Moin
Stanford University

Abstract

We discuss development of a numerical algorithm, and solver capable of performing large-eddy simulation (LES) in geometries as complex as the combustor of a gas-turbine engine. The algorithm is developed for unstructured grids, is non-dissipative, yet robust at high Reynolds numbers on highly skewed grids. Results from validation in simple geometries is shown along with simulation results in the exceedingly complex geometry of a Pratt & Whitney gas turbine combustor.

1 Introduction

The Navier-Stokes equations for incompressible flow are

$$\frac{\partial u_i}{\partial t} + \frac{\partial u_i u_j}{\partial x_j} = -\frac{\partial p}{\partial x_i} + \nu \frac{\partial^2 u_i}{\partial x_j x_j}; \qquad \frac{\partial u_i}{\partial x_i} = 0. \tag{1}$$

Large-eddy simulation (LES) is a computational approach where one filters the unsteady Navier-Stokes equations in space, and then numerically solves for the large-scales of motion, while modeling the effect of the filtered scales. Assuming that the spatial filter commutes with the spatial and temporal derivatives, the LES equations for the filtered velocity and pressure are

$$\frac{\partial \overline{u}_i}{\partial t} + \frac{\partial \overline{u}_i \overline{u}_j}{\partial x_j} = -\frac{\partial \overline{p}}{\partial x_i} + \nu \frac{\partial^2 \overline{u}_i}{\partial x_j x_j} + \frac{\partial \tau_{ij}}{\partial x_j}; \qquad \frac{\partial \overline{u}_i}{\partial x_i} = 0. \tag{2}$$

where $\tau_{ij} = \overline{u_i u_j} - \overline{u}_i \overline{u}_j$ is the subgrid stress, and is modeled.

There is considerable general incentive to develop LES on unstructured grids. However, LES on unstructured grids requires development of the appropriate numerical methods. Specifically, the numerical methods used to solve the RANS equations are not directly applicable to LES. RANS typically uses upwinded numerical methods; upwinding provides numerical dissipation, which makes the solution-procedure robust. However, when used for LES, upwinding severely compromises accuracy (e.g. Mittal & Moin 1997), since the numerical dissipation competes with, and often overwhelms the physical dissipation of the subgrid model.

By definition, the dissipative scales are not resolved by the grid in a LES. In practice this leads to numerical instability if straight-forward non-dissipative central-difference schemes are used. One solution to this problem is to develop non-dissipative numerical schemes that discretely conserve not only first order quantities such as momentum, but also second - order quantities such as kinetic energy (e.g. Arakawa 1963, Fromm & Harlow 1963, Lilly 1965, Mansour et al.

1979). Discrete energy conservation ensures that the flux of kinetic energy, $\sum_{\text{cvs}} u_i \partial(u_i u_j)/\partial x_j$ only has contributions from the boundary faces. This makes the solution robust without the use of numerical dissipation. Note that satisfying one constraint discretely, does not ensure the other - both constraints have to be simultaneously enforced when deriving the algorithm. The Harlow-Welch algorithm (1965) possesses this property on *structured* grids, and has therefore been widely used for LES on structured grids in simple geometries. We have developed a numerical method suitable for LES on unstructured grids that has been implemented on massively parallel computers (Mahesh et al. 1999, 2000, 2001). The development was evolutionary and is summarized below. First, the Harlow-Welch formulation was generalized to unstructured grids using a rotational form of the convection terms. While elegant, this formulation was found lacking when extended to three-dimensions. In particular its restriction to tetrahedral elements, and lack of robustness on skewed grids were serious limitations. An alternative formulation was therefore derived which can be applied to arbitrary elements. Robust yet accurate solutions are now obtained at high Reynolds numbers in very complex geometries on highly skewed grids. Details follow.

2 Staggered rotational formulation

We describe below the spatial discretization of the two-dimensional incompressible Navier-Stokes equations on an unstructured grid of triangles. The formulation is a conceptual extension of the popular staggered formulation on structured grids [**?**]. Figure **??** shows a single triangular element. Note that the pressure is stored inside the element (at the circumcenter), while the velocities normal to the edges of the triangle are stored at the edge-centers.

Denoting the edge-normal velocity by v_n, we have:

$$\frac{\partial v_n}{\partial t} - (\vec{u} \times \vec{\omega}) \cdot \vec{n} + \frac{\partial}{\partial n}\left(\frac{\vec{u} \cdot \vec{u}}{2}\right) = -\frac{1}{\rho}\frac{\partial p}{\partial n} + \nu \left(\nabla^2 \vec{u}\right) \cdot \vec{n} \tag{3}$$

We have $\nabla^2 \vec{u} = -\nabla \times \vec{\omega} + \nabla\left(\nabla \cdot \vec{u}\right)$. Also in two dimensions, $(\vec{u} \times \vec{\omega}) \cdot \vec{n} = \omega v_t$.

If the velocity field is divergence-free, this implies that $\left(\nabla^2 \vec{u}\right) \cdot \vec{n} = -\frac{\partial \omega}{\partial s_t}$. where $\frac{\partial}{s_t}$ denotes the tangential derivative. To time-advance the momentum equation, we therefore need the vorticity at the nodes and the edge-centers, tangential velocity at edge centers, total kinetic energy and pressure at the cell-centers.

The vorticity at the nodes is computed using Green's theorem i.e. $\int_A \omega \mathrm{d}A = \int_C \vec{u} \cdot \mathrm{d}\vec{l}$. The area over which the integration is performed is shown in figure **??**, and is obtained by joining the circumcenters of the triangles that surround the node. It is easily seen that the velocity components parallel to the edges of this area are normal to the edges of the triangles that make up the area. The vorticity at the node 'n' is therefore computed as $\omega = \frac{1}{A_{\text{dual}}} \sum_{\text{edges}} v_n l_{\text{edges}}$. where the length of the edges of the dual mesh is the distance between the circumcenters of the triangles that constitute the dual mesh.

Once the nodal vorticities are known, the vorticity at the edge-centers may be computed as the average of the vorticity at the corresponding nodes. Also the tangential derivative of the vorticity at the edge-center may be computed as the difference of the nodal vorticities divided by the edge length. These approximations are second-order accurate in the edge length. The tangential velocities at the edges are obtained by interpolating from neighboring edges. A fractional step approach for the pressure is derived as follows. Denote the nonlinear terms by NL and the viscous terms by V, and use the Adams-Bashforth method for both. Ignoring pressure in the first fractional step, we get

$$\frac{\widehat{v} - v_n^k}{\Delta t} = \frac{1}{2}\left[3(NL+V)^k - (NL+V)^{k-1}\right] \tag{4a}$$

$$\frac{v_n^{k+1} - \widehat{v}}{\Delta t} = -\frac{\partial \phi^{k+1}}{\partial n}. \tag{4b}$$

We require that the divergence of the velocity field at t_{k+1} be zero; i.e $A_v \nabla \cdot \vec{u} = \sum_e v_{ne} l_e. = 0$. Equation **??** therefore implies that

$$\frac{1}{\Delta t} \sum_e v_n^{n+1} l_e - \frac{1}{\Delta t} \sum_e \widehat{v} l_e = -\sum_e \frac{\partial \phi^{n+1}}{\partial n} l_e, \tag{5}$$

which along with the continuity constraint requires that the potential ϕ satisfy

$$\sum_e \frac{\partial \phi^{n+1}}{\partial n} l_e = \frac{1}{\Delta t} \sum_e \widehat{v} l_e. \tag{6}$$

Since ϕ is stored at the circumcenter of the volume, its gradient normal to the edge is easily computed. This yields a set of discrete equations for ϕ that are then solved. These discrete equations are of the form,

$$c(i)\phi(i) + \sum_{j=1}^{3} c(i,j)\phi(j) = \text{rhs}(i) \tag{7}$$

where the sum over j is a sum over the three volumes that are neighbors of volume, 'i'. Equation **??** is easily written for the interior volumes. However, when it is applied to a boundary volume, it appears that the gradient of ϕ at the boundary is required. However this is not the case (see e.g. Moin & Kim 1980); this requirement can be circumvented as follows. The divergence-free condition requires that

$$\sum_{j=1}^{3} v_{ne} l_e = 0; \quad \text{i.e.} \quad \sum_{\text{interior edges}} v_{ne} l_e = -v_{nb} l_{eb}. \tag{8}$$

This implies that the pressure equation for the boundary elements may be obtained by summing equation **??** over the interior edges alone, and using equation **??** to relate the interior sum of the velocity to the normal velocity at the boundary; i.e.

$$\sum_{\text{interior edges}} \frac{\partial \phi^{n+1}}{\partial n} l_e = \frac{1}{\Delta t} \sum_{\text{interior edges}} \widehat{v} l_e + \frac{1}{\Delta t} v_{nb} l_{eb}. \tag{9}$$

This eliminates the need for boundary conditions on ϕ.

2.1 Validation

We consider the steady laminar flow in a two-dimensional driven cavity at a Reynolds number of 5000. Results from Ghia et al. (1982) are used for validation in figure **??**. The quantities validated include velocity profiles, the vorticity at the center of the primary vortex, and visualization of velocity vectors. The unstructured grid is seen to allow fewer points to be used; at a Reynolds number of 5000, comparable results were obtained using 10576 nodes (30925 triangles) as compared to 66049 nodes (65536 Cartesian elements) in Ghia et al's computations. No attempt was made to optimize the unstructured grids.

2.2 Extension to three-dimensions

The algorithm is extended to tetrahedral elements as follows. The pressure and any scalars are stored at the circumcenter of the tetrahedron. The velocity component normal to each face,

v_n is stored at the circumcenter of each face. The convection term is computed in rotational form as $(\vec{u} \times \vec{\omega}) \cdot \vec{n} = u_t \cdot (\omega_t \times \vec{n})$. v_t is obtained by interpolating from the neighboring faces, and there are two steps to obtaining the vorticity components in the plane of each face. First, the circulation theorem is invoked to obtain the vorticity along each edge of the face. This vorticity is then projected along the tangential basis vectors on the face, and averaged to obtain ω_t at the face circumcenter. The circulation theorem is applied on a closed circuit around each edge. This circuit is obtained by joining the circumcenters of the tetrahedra to which this edge belongs. This is made possible by the fact that the property of the circumcenter that all such segments will lie in the same plane. The circulation theorem $A_{\text{dual}}\omega = \sum_{\text{dual edges}} v_n l_{\text{edges}}$ yields the vorticity component along the edge. The edge-vorticities are interpolated to obtain the tangential vorticity components at the face circumcenter. The viscous term is obtained from the edge-vorticities using the identity, $A_{\text{face}} \left(\vec{\nabla} \times \vec{\omega}\right) \cdot \vec{n} = \sum_{\text{edges}} \omega l_{\text{edges}}$, where ω is the vorticity component along the edges previously computed, and l_e denotes the length of the edges of the face.

2.3 Problems with formulation

While elegant, the above formulation has some limitations. It is restrictive in that pressure (and scalars if any) is stored at the circumcenter of the triangular elements. This restricts the grid to elements whose circumcenter lies within them. For example, in two-dimensions, consider right-triangles. Their circumcenter lies on the hypotenuse, making it impossible to determine the pressure gradient normal to the hypotenuse. Highly skewed elements are another source of problem since the circumcenter will now lie outside the element. Although projection of the velocity field is still possible in this situation, the inaccurate computation of the pressure gradient is cause for concern.

Another more fundamental limitation concerns the restriction of the algorithm essentially to tetrahedra. While well-suited to grid very complex geometries, experience shows that hexahedral elements are better suited for unsteady computations since (i) hexahedral elements are more easily aligned with flow gradients such as boundary layers, and (ii) it takes fewer hexahedral elements to fill space than comparable tetrahedra. For example, a three-dimensional grid generated for a Pratt and Whitney gas-turbine combustor required a tetrahedral grid with approximately 600000 nodes and 6.35 million faces (normal velocities to be solved) while a hexahedral grid with only 1.5 million nodes and faces yielded significantly higher resolution near the walls.

3 Non-staggered formulation

An alternative approach was therefore derived. The basic idea is that the robustness at high Reynolds numbers is determined essentially by the convection term, while robustness on skewed grids is determined by both convection and the pressure gradient term. A formulation is derived that emphasizes energy conservation for the convection term on arbitrary grids. Accordingly, the cell velocities u_i and the face-normal velocities v_n are treated as essentially independent variables. This storage is similar to that used by Rhie & Chow (1983) to suppress odd-even decoupling in a colocated formulation. It is readily shown that the passive scalar equation,

$$\frac{\partial \phi}{\partial t} + \frac{\partial}{\partial x_i}\phi u_i = 0 \quad \Rightarrow \quad \frac{\partial \phi^2}{\partial t} + \frac{\partial}{\partial x_i}\phi^2 u_i = 0. \tag{10}$$

if the velocity field is divergence-free. Integrating the first equation in **??**, we get $V\frac{\mathrm{d}\phi_{\text{cv}}}{\mathrm{dt}} + \sum_{\text{faces}} \phi_{\text{face}} v_N A_f = 0$ where V denotes the cell volume. This discrete equation has the same conservative property for ϕ^2 if $\phi_{\text{face}} = (\phi_{\text{icv1}} + \phi_{\text{icv2}}/2)$ and $\sum_{\text{face}} v_N A_f = 0$. This observation is

extended to the Navier-Stokes equations by computing the convection term in a similar manner. Note that the symmetry of the interpolation is retained even on non-uniform grids. This makes the solution robust on skewed grids since the discretization does not 'see' the underlying rough grid. As the results will show, this robustness results in no visible degradation of accuracy.

The convection term computed in the above manner yields a predicted value for the cell-velocities $\widehat{u}_i$. These predicted velocities are interpolated to obtain a prediction for the face-normal velocities $\widehat{v}$. The face-normal velocities are projected using $v_N - \widehat{v} = -\frac{\partial \phi}{\partial N}$ and ϕ is obtained from the discrete Poisson equation that results. The gradient of ϕ at the cell-centers is then used to update the cell velocities; i.e. $u_i = \widehat{u}_i - \frac{\partial \phi}{\partial x_i}$.

It turns out that the details of how $\frac{\partial \phi}{\partial x_i}$ are computed, affect the robustness of the solution on highly skewed grids. An obvious approach to computing the gradient at cell-centers is to use the gradient theorem; $\frac{\partial \phi}{\partial x_i} = \frac{1}{V} \sum_{\text{faces}} \phi_{\text{face}} A_f N_i$. When applied to flows such as homogeneous turbulence, turbulent channel flow and even a coaxial combustor for which the grids are very regular, very accuracet results are obtained. However when applied to highly skewed grids such as those in the Pratt & Whitney combustor, unstable solutions are obtained. This behavior is found at both high and low Reynolds numbers, pointing to the pressure-gradient as the source of the problem. It is readily seen that for a staggered formulation,

$$\sum_{\text{cvs}} \sum_{\text{faocv}} v_N^f \left(\phi_{\text{nbr}} - \phi_{\text{cv}}\right) A_f = \text{boundary terms} \tag{11}$$

However,

$$u_i - \widehat{u}_i = -\frac{\partial \phi}{\partial x_i} \quad \Rightarrow \quad \sum_{\text{cvs}} u_i \sum_{\text{faocv}} \left(\frac{\phi_{\text{cv}} + \phi_{\text{nbr}}}{2} \right) N_i A_f \quad = \quad \sum_{\text{cvs}} \frac{u_{\text{cv}}}{2} \sum_{\text{faocv}} \phi_{\text{nbr}} A_f N_i \tag{12}$$

This is because pressure is not obtained by taking the discrete divergence of the above equation; doing so will result in odd-even decoupling. As a result, $\frac{1}{2}\left(\frac{\partial \phi_{\text{icv1}}}{\partial x_i} + \left(\frac{\partial \phi_{\text{icv2}}}{\partial x_i}\right) N_i \neq \frac{\partial \phi}{\partial N}\right.$ at the faces. The pressure gradient term is therefore no longer discretely energy conserving. We therefore developed the following solution. Once ϕ is known, $\frac{\partial \phi}{\partial x_i}$ is computed such that for each cell, $\frac{\partial \phi}{\partial x_i N_i^{\text{faces}}}$ equals $\frac{\partial \phi}{\partial N}$ in a least squares sense. The resulting algorithm is found to be both robust on highly skewed grids as well as accurate.

3.1 Results

3.1.1 Taylor problem

Figure **??**, shows the evolution of kinetic energy in the Taylor problem - an analytical solution, which describes counter-rotating vortices that decay in time. Our formulation is compared to a non-dissipative formulation that only conserves momentum. Both formulations have the same computational stencil. At low Reynolds numbers, where the dissipative scales are resolved, both formulations are stable, although our formulation shows better agreement with the analytical result. However, at very high Reynolds numbers where the dissipative scales are not resolved, the formulation that does not conserve kinetic energy becomes unstable after some time, while our formulation is seen to essentially maintain its initial kinetic energy as required by the analytical solution.

3.1.2 Flow in a coaxial combustor

Results are shown for the turbulent flow in a coaxial combustor configuration at conditions corresponding to experiments by Sommerfeld & Qiu (1991, 1992, 1993). The chamber consists

of central core (primary) and annular (secondary) jets discharging into a cylindrical test section with sudden expansion. The primary jet has a radius of 16 mm and the secondary annular jet extends over the radial interval of 19-32 mm. The outer radius of the annulus is 32 mm, the test-section is 960 mm long, and flow in the annular section has mean swirl. The Reynolds number of the primary jet is 26200 and the swirl number in the annulus is 0.47.

The computational domain is divided in $\sim 1.6 \times 10^6$ hexahedral volumes, with $\sim 0.9 \times 10^6$ elements clustured in the first half of the test section. The smallest grid spacing is ~ 32 μm near the walls and in the shear layers close to the annular inlet into the test section. Profiles at six stations of mean streamwise, radial and azimuthal velocities and turbulence kinetic energy were compared to experiment and very good agreement was observed. Only turbulence kinetic energy is shown in figure **??**; the other results are reported by Mahesh et al. (2001).

3.1.3 Pratt & Whitney gas turbine combustor

Simulations were performed in the exceedingly complex geometry of the combustor in a Pratt & Whitney gas-turbine engine. The geometry was provided in IGES format. Experimental data for mass-splits and pressure drop across the injector was used for validation. Figure **??** illustrates the geometry; the level of complication is apparent. The Reynolds number in the pre-diffuser based on the bulk velocity and cross-section was $500,000$; values in in the main (core) swirler channel were 150000. Turbulent fluctuations from a separate calculations in a pipe sector of identical shape as the pre-dif fuser inlet section were fed at the inlet. Table **??** compares LES predictions of the flow splits to experiment; good agreement is observed.

Location	LES Error % wrt expt.	LES Error % wrt inlet
OD dilution hole	3.1	0.8
ID dilution hole	3.5	0.5
Core (main swirler)	10.3	0.14
Second (OD) swirler	7.5	0.35
Third (Guide) swirler	0.4	0.02

Table 1: Comparison to experiment of mass flow splits in the Pratt & Whitney combustor geometry

4 Summary

We have discussed development of a numerical algorithm, and solver capable of performing large-eddy simulation (LES) in geometries as complex as the combustor of a gas-turbine engine. The algorithm is developed for unstructured grids, has non-dissipative convection, and yet robust at high Reynolds numbers on highly skewed grids. Results from validation in simple geometries is shown along with simulation results in the exceedingly complex geometry of a Pratt & Whitney gas turbine combustor.

Acknowledgements

We are immensely grateful to Mr. Gianluca Iaccarino for his assistance in generating the grid used in the combustor simulations, and to Dr. Sourab Apte for useful discussions. This work was supported by the DOE under the Accelerated Strategic Computing Initiative at Stanford University.

References

[1] Arakawa, A., 1966, Computational design for long term numerical integration of the equations of fluid motion: two-dimensioanl incompressible flow, Part I, *J. Comp. Phys.*, 1: 119–143.

[2] Fromm, J.E. & Harlow, F.H., 1963, Numerical solution of the problem of vortex street development, *Phys. Fluids*, 6:175–182.

[3] Ghia, U, Ghia, K.N. & Shin, C.T., 1982, High-Re solutions for incompressible flow using the Navier-Stokes equations and a multigrid method. *J. Comp. Phys.* 48: 387-411.

[4] Harlow, F.H. & Welch, J.E., 1965, Numerical calculation of time-dependent viscous incompressible flow of fluid with free surface. *Phys. Fluids* 8: 2182-2189.

[5] Lilly, D.K., 1965, On the computational stability of numerical solutions of time-dependent non-linear geophysical fluid dynamics problems, *Monthly Weather Review*, 93:11–26.

[6] Mahesh, K. & Ruetsch, G.R. & Moin, P., 1999, Towards large–eddy simulation in complex geometries, *Annual Research Briefs - 1999*, pp. 379–387.

[7] Mahesh, K., Constantinescu, G. & Moin, P., 2000, Large–eddy simulation of gas–turbine combustors, *Annual Research Briefs - 2000*, pp. 219 – 228, Center for Turbulence Research, Stanford University.

[8] Mahesh, K., Constantinescu, G., Apte, S., Iaccarino, G. & Moin, P., 2001, Large–eddy simulation of gas-turbine combustors, *Annual Research Briefs - 2002*, pp. 3–17, Center for Turbulence Research, Stanford University.

[9] Mansour, N.N., Moin, P., Reynolds, W.C. & Ferziger, J.H., 1979, Improved methods for large-eddy simulation fo turbulence, *Proc. Turbulent Shear Flows I*, pp. 386-401, ed. F. Durst, B.E. Launder, F.W. Schmidt & J.H. Whitelaw, Springer, Berlin.

[10] Mittal, R. & Moin, P., 1997, Suitability of upwind biased schemes for large-eddy simulation, *AIAA J.*, **30:8** 1415–1417.

[11] Moin, P. & Mahesh, K., 1998, Direct numerical simulation: a tool in turbulence research, *Ann. Rev. Fluid Mech.*, **30:** 539–578.

[12] Pierce, C.D. & Moin, P., 2001, Progress variable approach for large eddy simulation of turbulent combustion. *Report TF - 73*, Mechanical Engineering Dept., Stanford University, Stanford, California.

[13] Rhie, C.M. & Chow, W.L., (1983) A numerical study of the turbulent flow past an isolated airfoil with trailing edge separation. *AIAA J.* 21:1525–1532.

[14] Sommerfeld, M. & Qiu, H.H., 1991, Detailed measurements in a swirling particulate two -phase flow by a phase - doppler anemometer. *Int. J. of Heat and Fluid Flow* 12(1):20-28.

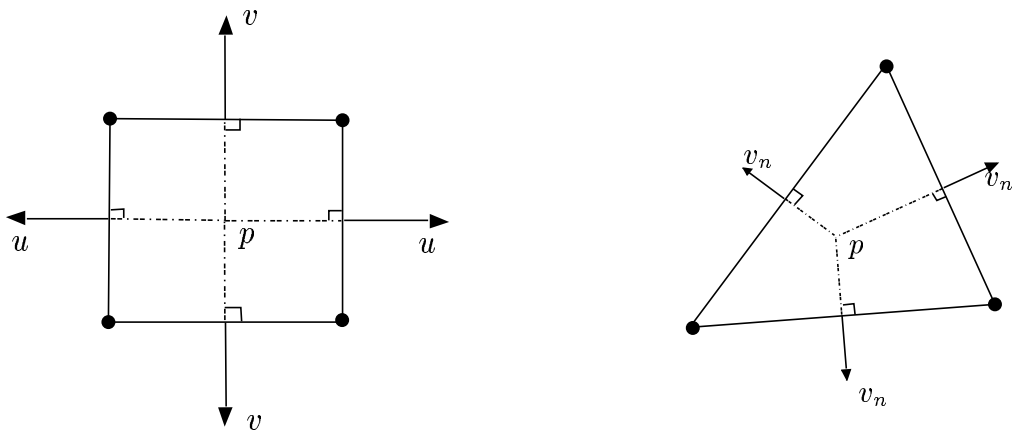

Figure 1: The staggered positioning of variables on an unstructured mesh of triangles is contrasted with that on a structured mesh.

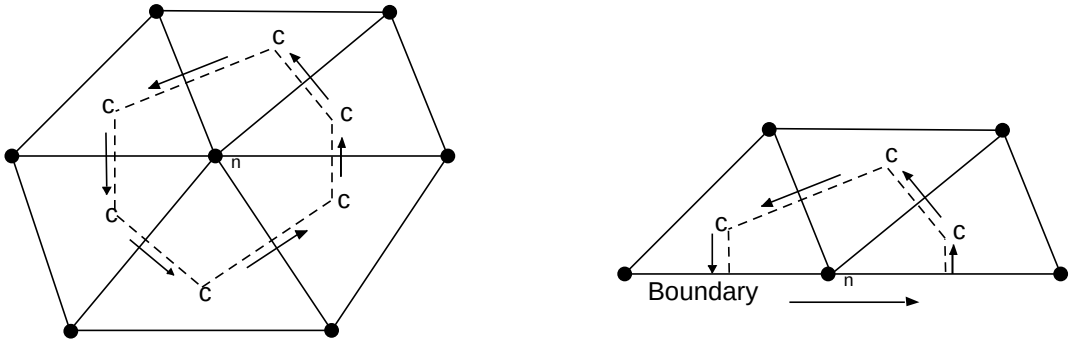

Figure 2: Illustration of the dual mesh used to compute the vorticity at the nodes.

Interior node

Boundary node

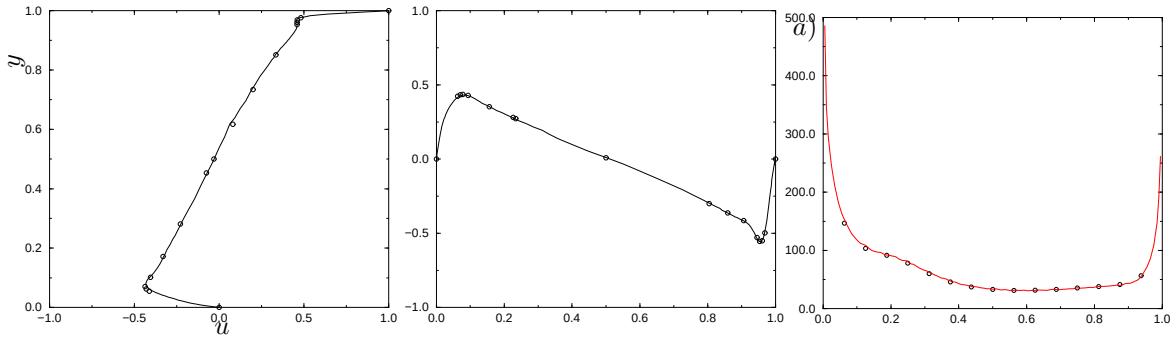

Figure 3: Unstructured results (solid lines) are compared to results from Ghia et al. (symbols). The Reynolds number is 5000. (a) Vertical profile of streamwise velocity at $x = 0.5$. (b)Streamwise profile of vertical velocity at $y = 0.5$ (c) vorticity at the top boundary.

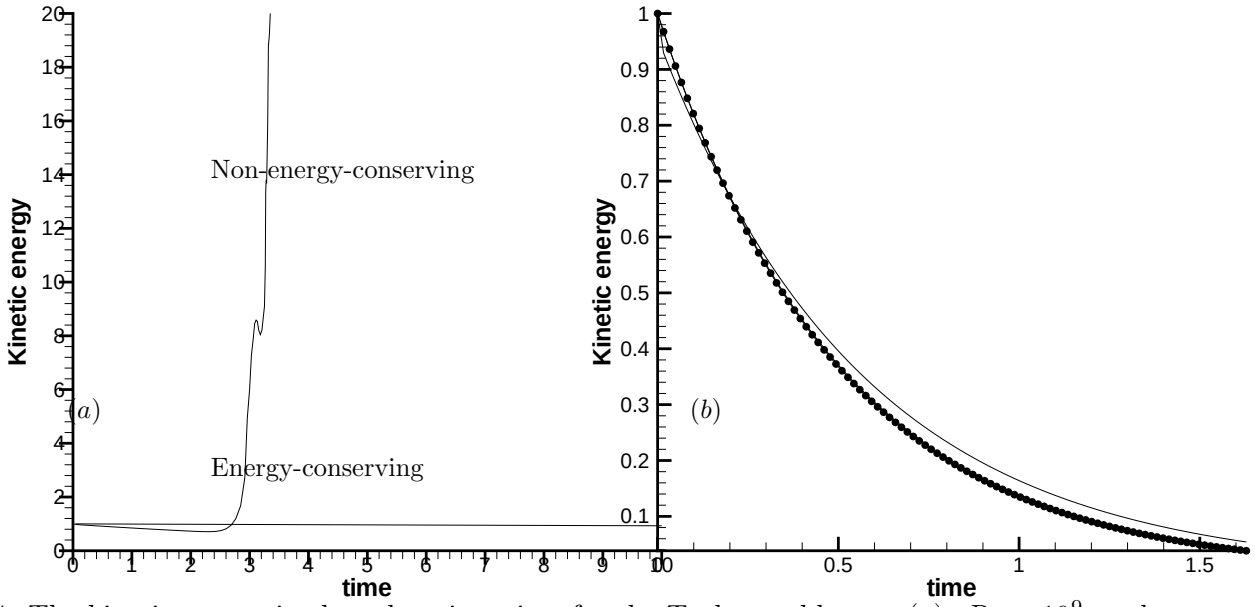

Figure 4: The kinetic energy is plotted against time for the Taylor problem at (a): $Re = 10^9$, and (b): $Re = 1$. At the lower Reynolds number, both schemes are stable. At higher Reynolds number, only the energy-conserving scheme is stable. The solid circles in (b) denote the analytical solution; the energy-conserving formulation passes through them.

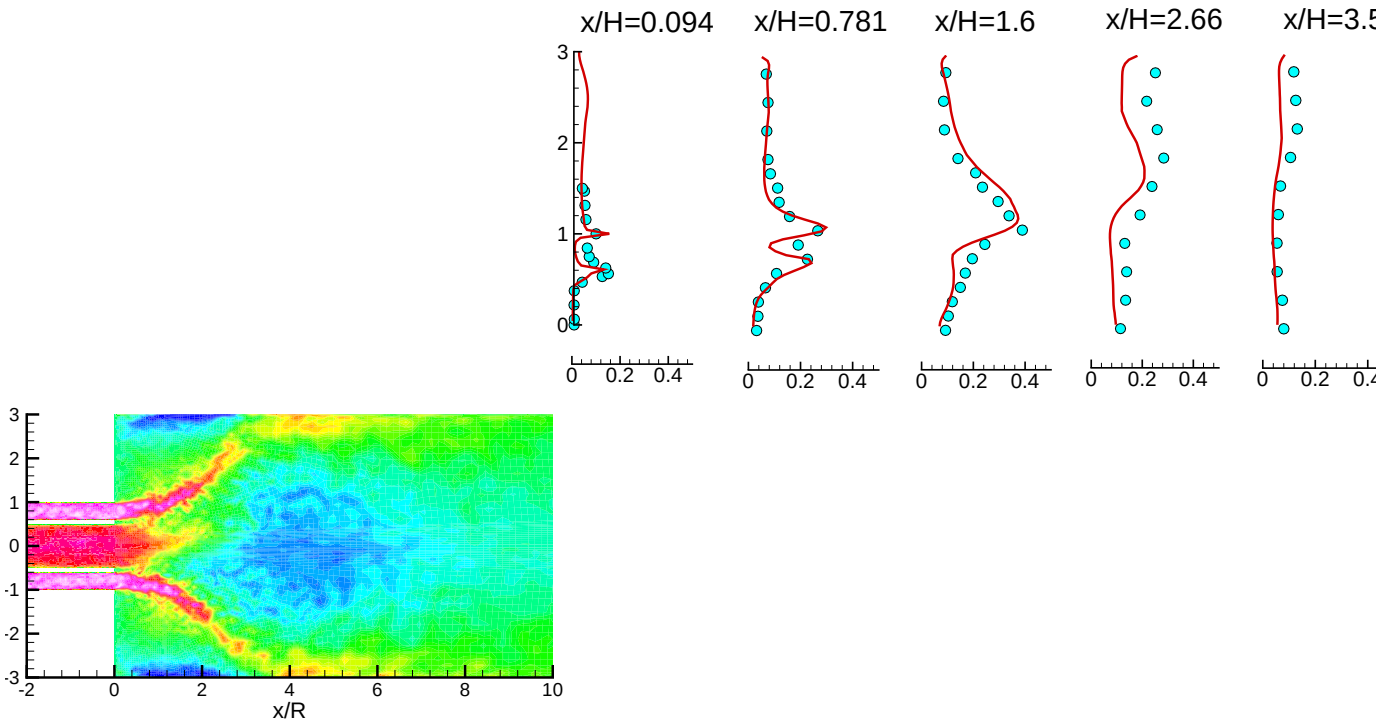

Figure 5: Contours of axial velocity and profiles of turbulent kinetic energy in LES of incompressible swirling flow in a coaxial combustor geometry. Conditions correspond to an experiment by Sommerfeld & Qiu(1991). Only part of the computational domain is shown for clarity.

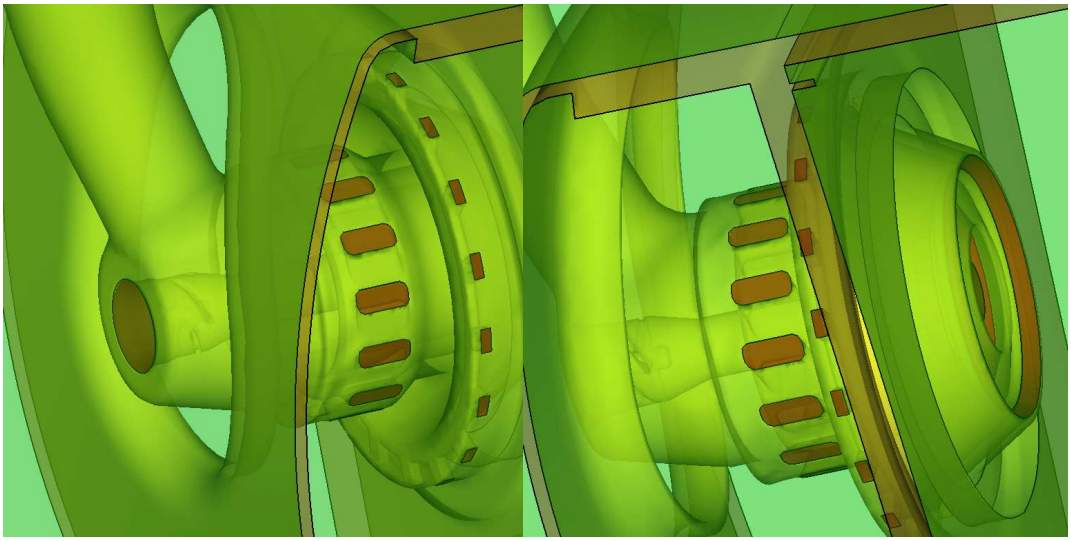

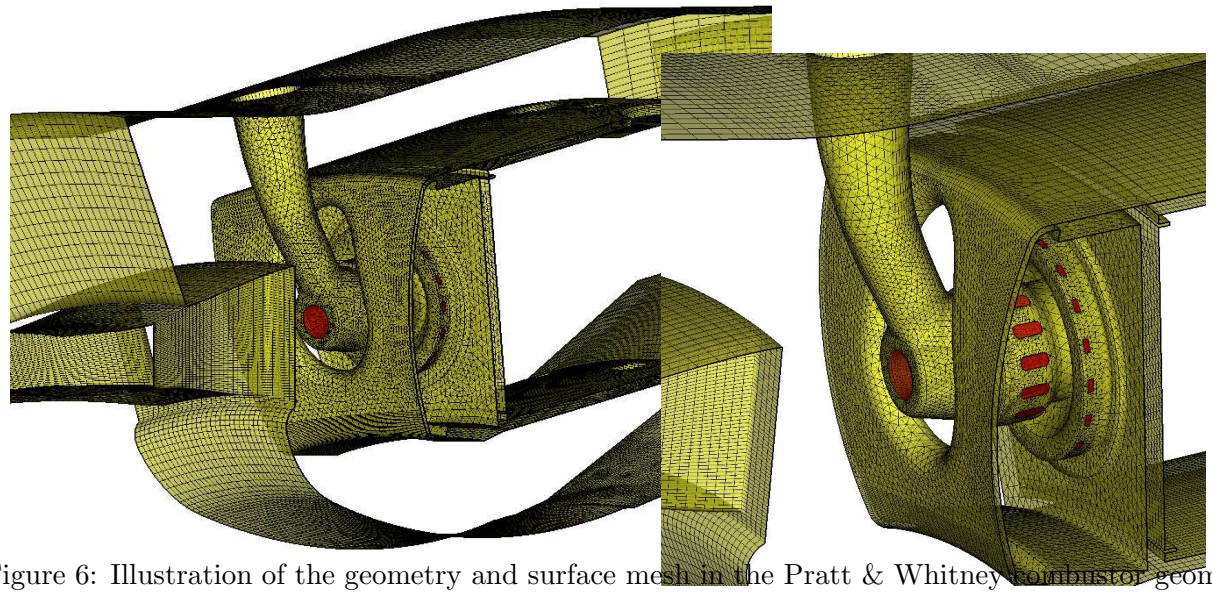

Figure 6: Illustration of the geometry and surface mesh in the Pratt & Whitney combustor geometry.

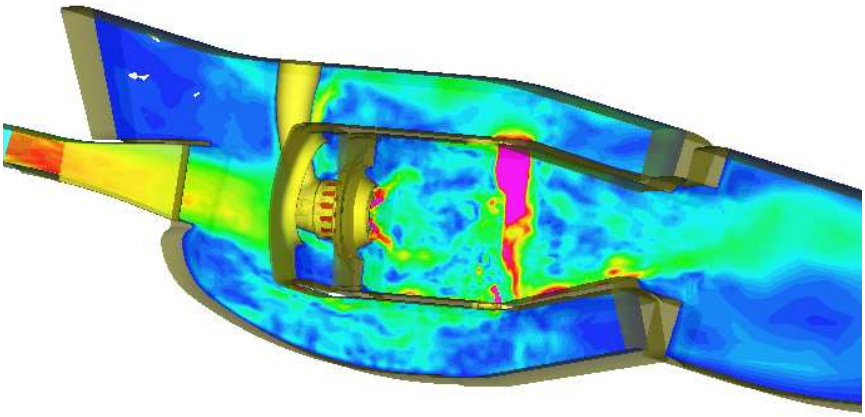

Figure 7: Instantaneous velocity magnitude contours in combustor geometry. Red corresponds to high velocities and blue to low velocities.